PHOTONICS Research

High-efficiency all-dielectric transmission metasurface for linearly polarized light in the visible region

Liu Yang,[1,†] Dong Wu,[1,†] Yumin Liu,[1,*] Chang Liu,[1] Zenghui Xu,[1] Hui Li,[1] Zhongyuan Yu,[1] Li Yu,[1,2] and Han Ye[1]

[1]State Key Laboratory of Information Photonics and Optical Communications, Beijing University of Posts and Telecommunications, Beijing 100876, China
[2]School of Science, Beijing University of Posts and Telecommunications, Beijing 100876, China
*Corresponding author: microliuyumin@hotmail.com

Received 15 January 2018; revised 20 March 2018; accepted 20 March 2018; posted 21 March 2018 (Doc. ID 319749); published 26 April 2018

We propose and numerically investigate an efficient transmission-mode metasurface that consists of quasi-continuous trapezoid-shaped crystalline silicon nanoantennas on a quartz substrate. This metasurface provides a linear phase gradient and realizes both full 2π phase shift and high transmission efficiency in the operating wavelength range from 740 to 780 nm. At the central wavelength around 751 nm, the total transmission efficiency is up to 88.0% and the section of the desired anomalous refraction is 80.4%. The anomalous refraction angle is 29.62°, and larger refraction angle can be achieved by changing the period of the super cell. We demonstrate a refraction angle as large as 38.59°, and the anomalous transmission efficiency reaches 76.6% at wavelength of 741 nm. It is worth mentioning that the structure is much simpler than conventional metasurfaces based on arrays of discrete nanoantennas. Our research may pave the way for designing efficient all-dielectric phase-gradient metasurfaces and applying them in integrated optical devices for wavefront control.

OCIS codes: (160.3918) Metamaterials; (050.5080) Phase shift; (230.3120) Integrated optics devices.

https://doi.org/10.1364/PRJ.6.000517

1. INTRODUCTION

In recent years, metasurfaces have gained more and more attention because of their remarkable features. Compared to conventional bulky metamaterials, metasurfaces are much more flexible to accurately tailor optical properties such as amplitude, phase, and polarization [1–5]. Also, metasurfaces are easier to fabricate and apply to integrated photonic systems as a kind of ultra-thin two-dimensional metamaterial. Since Yu *et al.* explained the generalized laws of reflection and refraction in detail and further proposed phase-gradient metasurfaces based on classical V-shaped antenna arrays [6], many similar structures exploiting discrete nanoantennas of various shapes have been numerically and experimentally investigated [7–24]. The applications include full-color printing [13], meta-holograms [11,14,15], polarization converters [16–18], flat lenses [19–23], optical vortex generation [3,6,23,24], and spectrum splitters [25–28].

More recently, all-dielectric metasurfaces have been widely studied because of their low loss and high efficiency in transmission mode [2,3,5,13,17,20]. Meta-based metasurfaces with high efficiency have been realized [29,30], but they work in reflection mode, which is not very convenient for some applications, such as polarization converters, metalenses and spectrum splitters, because it is hard to separate the incident and reflected light completely. High-efficiency meta-based transmission metasurfaces have also been proposed [31,32], but they work at long wavelengths, such as in the gigahertz wavelength region, where the loss of metal is much lower than in visible region. When working in transmission mode in the visible region, meta-based metasurfaces are lossy, as mentioned before. Compared to most metasurfaces involving plasmonic resonances, all-dielectric metasurfaces avoid the inherent loss of metals and greatly improve the efficiency [2,17,33]. Conventional structures based on arrays of discrete nanoantennas still face some problems, particularly precise fabricating difficulties and anomalous refraction angle limitations. The super cells of conventional metasurfaces usually contain several nanoantennas with varying geometric sizes and azimuth angles to gain a linear phase gradient, which makes precise reproduction very challenging [1,7–12,18]. To simplify the structure, some research groups adopted rectangular or circular posts with different section side lengths or diameters [2,3,13,21–23]. However, those dielectric posts usually need high aspect ratios to gain phase shift and high transmission efficiency, particularly for visible light manipulating, which also complicates the

fabrication. When using lossless but lower refractive index materials like titanium dioxide (TiO_2) [13,21,22] and silicon nitride (Si_3N_4) [23] to improve the transmission efficiency, the required aspect ratios are even as high as 10–15 and 6 [2]. Reducing the aspect ratio and guaranteeing high transmission efficiency at the same time are key problems of designing metasurfaces. Zhou *et al.* designed a metasurface that consists of a graded array of silicon posts with an aspect ratio of 3.4 arranged in a square lattice on a quartz substrate, which enables full 2π control at the wavelength of 532 nm, and the transmission efficiency reached 71% [2]. However, there are still eight units in one super cell, and the operating wavelength is limited in a narrow bandwidth around the central wavelength of 532 nm. In 2014, Li *et al.* proposed a new type of metasurface, known as a continuous metasurface, that has only one trapezoidal antenna within a super cell [34]. The work offered us a new idea in designing phase-gradient metasurfaces. Afterward, the group also demonstrated some applications utilizing continuous or quasi-continuous metasurfaces. However, their works focused mainly on plasmonic metasurfaces containing metals and operating in the visible light range in reflection mode [25,27]. As mentioned earlier, the loss of metals is inevitable and the efficiency is obviously affected. Another problem is that many metasurfaces suffer from limited anomalous refraction or reflection angles. The efficiency declines sharply when the angles turn larger.

To summarize, for phase-gradient metasurfaces, simple structure, high efficiency, and large anomalous deflection angle are required. In this work, we combine the advantages of both all-dielectric and quasi-continuous metasurfaces to realize high-efficiency anomalous refraction with a simple structure, overcoming the limitation of large aspect ratio. We design an all-dielectric quasi-continuous phase-gradient metasurface consisting of only one trapezoidal silicon antenna within a super cell on a quartz substrate. As we all know, silicon is widely used for its high refractive index and CMOS compatibility [2,3,35]. Although the imaginary part of the refractive index defined as the extinction coefficient of crystalline silicon exists in the visible light range, it is very small in operation wavelength range of 720–780 nm, so the material absorption is very low. Sell *et al.* realized efficient metasurface devices based on single crystal silicon nanoridges across the entire visible spectrum, ranging from 480 to 700 nm, and envisioned that crystalline silicon metasurfaces will enable compact optical systems spanning the full visible spectrum [36]. We demonstrate that high efficiency of about 80.5% of input energy is transmitted to the desired angle at a central operating wavelength of 751 nm, and the anomalous refraction angle reaches 29.62°. Larger anomalous refraction angle is also obtained by decreasing the period of the super cell. The calculated results show that the angle can be controlled by tailoring the geometrical parameters of the structure. We demonstrate an angle of 38.59° with a transmission efficiency about 76.7%. It is believed that this work will offer a new idea for designing all-dielectric metasurfaces for visible light. The designed metasurface can be applied to integrated optical devices such as flat lenses, waveplates, and beam expanders.

2. THEORY AND SIMULATION

A. Modeling and Design

To determine the geometrical parameters of the quasi-continuous trapezoid-shaped nanoantennas and explain the physical mechanism of the generation of the phase shift, we calculate a simple homogeneous metasurface composed of rectangular crystalline silicon posts based on silica film, which is shown in Fig. 1. Considering the actual fabrication, we add adhesive NOA61 and quartz substrate. The measured data from Palik are used to describe the refractive index of silicon [37], and the refractive index of NOA61 is 1.56 [2]. For both silica and quartz, the refractive index is 1.45. The period of the unit cell is $P = 190$ nm, and the height of the silicon post h is 290 nm. The thickness of each substrate layer is 1 μm. The wavelengths of the incident light are 500–900 nm. We change the cross-section length of the silicon post w and calculate the transmission and phase of the transmitted light.

Figure 2(a) shows the variation of phase and transmission by changing the cross-section length of the posts at the wavelength of 751 nm. We find that, when w changes from about 20 to

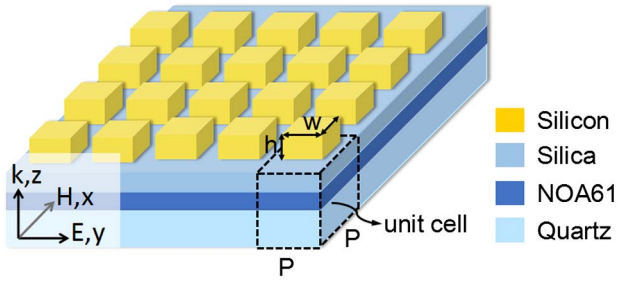

Fig. 1. Schematic of the homogeneous metasurface composed of rectangular crystalline silicon posts based on silica film.

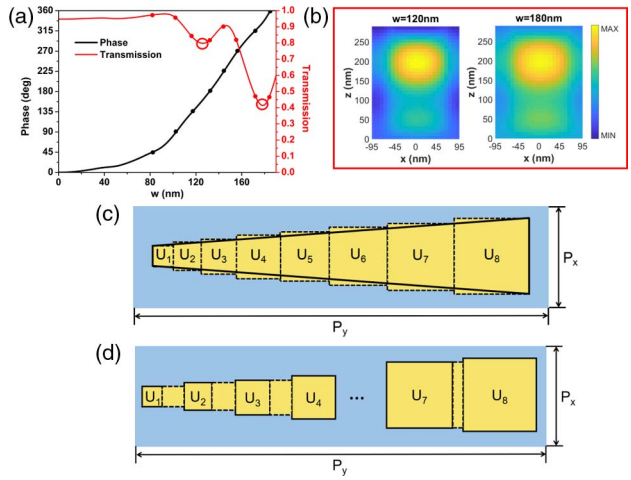

Fig. 2. (a) Transmission and phase of the periodic c-silicon posts with 190 nm unit cell size and 220 nm height for different cross-section lengths at the wavelength of 751 nm. (b) Magnetic field amplitudes in the x–z plane (H_{xz}) for $w = 120$ nm and $w = 180$ nm at wavelength of 751 nm. (c) Vertical view of the compactly arranged silicon posts. (d) Vertical view of the period formed by filling the gaps between the silicon posts.

Table 1. Cross-Section Lengths of the Silicon Posts

Unit cell (phase)	U_1 (45°)	U_2 (90°)	U_3 (135°)	U_4 (180°)	U_5 (225°)	U_6 (270°)	U_7 (315°)	U_8 (360°)
w (nm)	82	102	116	132	144	155	172	184

180 nm, a full 2π phase shift can be realized, and the transmission is high on the whole. We choose eight different cross-section length posts with $\pi/4$ increments to cover a full 0–2π phase shift. The cross-section lengths are shown in Table 1. There are two dips in the transmission line in Fig. 2(a) corresponding to $w = 120$ nm and $w = 180$ nm.

We calculate the magnetic field amplitudes in the x–z plane (H_{xz}) for $w = 120$ nm and $w = 180$ nm. The magnetic fields show Fabry–Perot-type resonances [2] in the posts, which lead to phase shift of the transmitted light. To make a quasi-continuous structure, we arrange the posts compactly from small to large and approximately form a quasi-continuous trapezoid-shaped nanoantenna, which is shown in Fig. 2(c), and another quasi-continuous structure formed by filling the gaps between the posts with silicon, which is shown in Fig. 2(d). We calculate the phase shift of the quasi-continuous structures shown in Figs. 2(c) and 2(d). The results show apparent differences compared to conventional metasurfaces based on arrays of discrete silicon posts. Because of the asymmetry of the trapezoidal nanoantennas, the quasi-continuous metasurfaces have polarization selectivity. Only the light with direction of polarization perpendicular to the direction of the phase gradient can produce a full 2π linear phase gradient. The results also show that the operation wavelength bands are moving. In addition, whether compactly arranging the posts or filling the gaps, a full 2π phase shift can be realized, which shows the flexibility of designing quasi-continuous metasurfaces. This may provide a new idea for designing all-dielectric transmission phase-gradient metasurfaces. We do not discuss this in detail due to the limited space.

To simplify the structure and gain the highest transmission efficiency, we optimize the geometrical parameters, and the final designed structure is shown in Fig. 3. To illustrate the details clearly, the real aspect ratio is not adopted. The metasurface consists of periodically arranged isosceles trapezoid silicon nanoantennas based on silica film. The period of the super cell is fixed as $P_x = 1520$ nm, $P_y = 190$ nm to realize full 2π phase control and gain the largest possible anomalous refraction angle (θ_r). The geometrical parameters of the super cell are shown in Table 2.

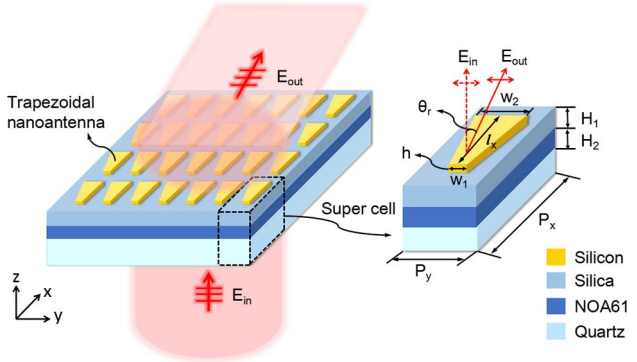

Fig. 3. Schematic of the proposed silicon phase-gradient metasurface composed of trapezoidal antenna arrays on a quartz substrate.

Table 2. Geometrical Parameters of the Designed Super Cell

Parameter	w_1	w_2	l_x	h	H_1	H_2
Value	82 nm	152 nm	887 nm	290 nm	1 μm	1 μm

B. Theoretical Basis

According to the generalized Snell law [6,38], the phase gradient along the horizontal direction at the interface between two media leads to anomalous refraction or reflection. For the condition of anomalous refraction, it is demonstrated as

$$n_r \sin\theta_r - n_i \sin\theta_i = \frac{\lambda_0}{2\pi}\frac{d\Phi}{dx}, \tag{1}$$

where θ_r and θ_i are the anomalous refraction angle and the incident angle, respectively, n_r and n_i are the refractive indices of the two media, λ_0 is the wavelength in free space, and $d\Phi/dx$ is the phase gradient. When considering only the condition that the surrounding medium is air and the light is incident normal to the interface, the equation could be simplified as

$$\sin\theta_r = \frac{\lambda_0}{2\pi}\frac{d\Phi}{dx} = \frac{\lambda_0}{P_x}, \tag{2}$$

where P_x is the period of the structure. For the proposed quasi-continuous metasurface, it is proved that the anomalous refraction angle could be described by the modified diffraction equation, which introduces the generalized Snell law [26] as

$$\sin\theta_r = m_0\frac{\lambda_0}{P_x} + \frac{\lambda_0}{2\pi}\frac{d\Phi}{dx} = (m_0+1)\frac{\lambda_0}{P_x}, \tag{3}$$

where m_0 is the traditional diffraction order. The desired anomalous refraction angle could be seen as the original zero-order diffraction shifted to the position of the first order.

We notice that the total number of all diffraction orders is decided by the operating wavelength and the period of the super cell. When λ_0/P_x is greater than 0.5, the value of m_0 could only be 0, and there will be only three diffraction orders: 0, +1, and −1.

When λ_0/P_x is less than 0.5 but greater than 1/3, m_0 could be 0 or 1, so there will be five orders: 0, +1, −1, +2, −2, and so on. The calculated results also prove this theory in the following discussion.

C. Simulation Methods

We perform the numerical calculation by using the finite-difference time-domain (FDTD) method and analyze the transmission efficiency and phase of the periodic isosceles trapezoid silicon nanoantennas. Periodic boundary conditions are used in the x and y directions, and perfectly matched layers are

exerted on boundaries in the z direction. The structure is illuminated by vertical incident linearly polarized plane light with the electric field polarized along the y direction, and the operating wavelength range is 720–780 nm. To illustrate the characteristics of the metasurface, we test mainly the transmission efficiency and the anomalous refraction angle; the total transmission and the transmission of the quartz substrate are defined as

$$T_{\text{out}} = I_{\text{out}}/I_s, \tag{4}$$

$$T_q = I_{tq}/I_s, \tag{5}$$

where I_{out} is the total transmission intensity, I_s is the total intensity of the input, and I_{tq} is the transmission intensity of the quartz layer. To make a clear comparison with previous research, we give out two kinds of definitions for efficiency of anomalous refraction, normalized to the input energy and the section of quartz layer's transmission intensity, respectively, as

$$\eta_{r1} = (I_r/I_s) \times 100\%, \tag{6}$$

$$\eta_{r2} = (I_r/I_{td}) \times 100\%, \tag{7}$$

where I_r is the desired anomalous refraction transmission intensity.

3. RESULTS AND DISCUSSION

A. Anomalous Transmission Properties

With the geometrical parameters of the super cell shown in Table 2, we test the phase of the transmission light. As shown in Fig. 4(a), the origin of coordinates is set at the center of the super cell. Through the super cell, a full 2π phase shift can be realized in the wavelength range of 740–780 nm. To make it clear, we select four wavelength points and plot the phase shift curves in Fig. 4(b). The phase shift at 751 nm wavelength is plotted with a black solid line, and we can gain the highest efficiency at this wavelength. The total transmission, reflection, and absorption are shown in Fig. 4(c). It is clear that the total transmission is up to 0.88 at the wavelength of 751 nm. The absorption is lower than 0.1 because the imaginary part of the refractive index of silicon is very small at this wavelength. The loss is caused mainly by the reflection. We set the monitors in the middle of the layers to test the transmission of quartz layer and silicon nanoantennas and make a comparison. We find that the reflection is almost entirely at the quartz–air interface, and the absorption is in the silicon nanoantennas. We plot the transmission of each layer in Fig. 4(d). It is obvious that the transmissions of the substrate and adhesive layers almost coincide, which means there is no loss inside the three layers. We calculate that the sum of the quartz layer's transmission and the reflection is 1, so we confirm that the reflection happens at the interface of quartz and air. The transmission curve of the silicon is in the middle of the two curves that represent quartz transmission and total transmission, which means the absorption occurs in the silicon layer.

We calculate the desired anomalous transmission efficiency at different wavelengths, and normalize it to the input energy and the transmission energy of quartz, which are plotted by the black and red solid lines, respectively. When normalized to the transmission energy of quartz, the reflection is not taken into account, so the calculated efficiency is significantly higher. We mainly take the efficiency that is normalized to the input energy as the performance index. As is shown in Fig. 5(a), the

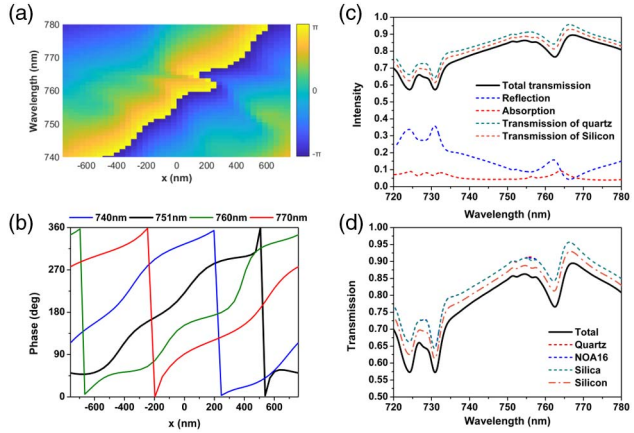

Fig. 4. Simulated phase and the electric field amplitude variation for silicon nanoantenna thickness $h = 290$ nm. (a) Simulated phase variation along the x direction of the super cell for wavelengths of 740–780 nm; (b) full 2π phase shift along the x direction of the super cell for typical wavelengths of 740, 751, 760, and 770 nm; (c) intensity of the transmission, reflection, and absorption; and (d) the transmission of every layer of the metasurface.

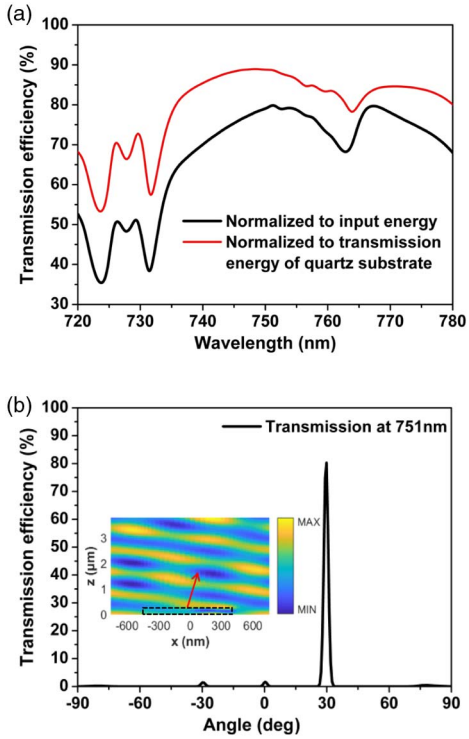

Fig. 5. (a) Simulated transmission efficiency normalized to input energy and the transmission energy of the quartz substrate for wavelengths of 740–780 nm. (b) Far-field transmission efficiency (normalized to input energy) for different anomalous refraction angles (θ_r) at wavelength of 751 nm, where the inset shows the E-field (E_y) distribution for the refracted light with the propagation being signified by a red arrow at wavelength of 751 nm.

transmission efficiency of the desired anomalous refraction is above 70% through 740–780 nm of wavelength range, and at 751 nm it is up to 80.4%.

According to Eq. (3), the transmission angle θ_r can be calculated by

$$\theta_r = \arcsin\left[(m_0 + 1)\frac{\lambda_0}{P_x}\right]. \quad (8)$$

At 751 nm of operating wavelength, the calculated angle of the +1 diffraction order is 29.62°, and the simulation result is consistent with the calculation results, which is shown in Fig. 5(b). The inset shows the electric field (E_y) of the transmission light at wavelength of 751 nm, and the characteristics of the plane wavefront can be clearly observed. To verify the relationship of the number of diffraction orders and the ratio of the wavelength to the period, which is described in Section 2, we test several refraction angles at different wavelengths and make a comparison with the theoretical calculation results in Table 3. The simulation results are highly consistent with that calculated by Eq. (8).

To study the performance of the structure in near-infrared band, we adjust the geometric parameters of the trapezoid structure according to the generalized law of refraction. The results show that in the wavelength range from 800 to 1200 nm, the total transmission of the structure remains above 70%, while the refraction is less than 20%. The absorption of the structure is very low and can be ignored. When the wavelength is near 820 nm, the efficiency of anomalous refraction is about 75%. However, this efficiency shows a decreasing tendency, while the transmission of the vertical projection becomes higher with the increase of wavelength.

According to the generalized law of refraction, which is shown in Eq. (2), the period (P_x) is closely related to the anomalous refraction angle (θ_r). In theory, the length range of the period can be λ_0 (the operating wavelength) to infinity. However, when the period becomes too large, the anomalous refraction angle is going to be very small and the anomalous refraction light will almost coincide with the vertical transmission light. In this case, the metasurface will lose its function of anomalous refraction. When the period is close to λ_0, the anomalous refraction angle will be large and the anomalous refraction transmission efficiency tends to decline. We calculate the two limiting cases in which the designed metasurface can keep its function, and the operating wavelength (λ_0) range is 730–760 nm. The results show that when the period (P_x) is adjusted to $1.18\lambda_0$–$5.68\lambda_0$, in which the anomalous refraction angle is in the range from 60° to 10°, the metasurface can keep its function, and the highest anomalous refraction transmission efficiency is above 50%. When the period is beyond this range, the metasurface will mainly lose its function of anomalous refraction. We discuss large anomalous refraction angles in more detail in Section 3.C.

Table 3. Calculation and Simulation Angles for All Diffraction Orders without 0 Order and Negative Angle of Symmetry

λ_0 (nm)		741	751	766	768
λ_0/P_x		0.4875	0.4941	0.5039	0.5053
Calculation	1 order	29.1877	29.6241	30.2587	30.3518
angle (°)	2 order	77.2506	81.3458	—	—
Simulation	1 order	29.1877	29.6241	30.2587	30.3517
angle (°)	2 order	77.2505	81.3458	—	—

B. Influence of the Thickness *h*

In the process of simulation and optimization, the results show that the thickness of the silicon nanoantennas has a certain influence on the transmission efficiency. As the thickness h increases, the transmission efficiency shows a tendency to slowly increase until reaches a maximum value and then decline, and, finally, it is lower than 50% at $h = 600$ nm. The optimal thickness where we can gain the highest transmission efficiency is 290 nm.

To investigate this phenomenon, we test the transmission, reflection, and absorption of the periodic silicon rectangular posts on the same substrate, which are shown in Fig. 6(a). We change the thickness h from 200 to 400 nm, while $P_x = P_y = 190$ nm, and the square cross-section length is 100 nm unchanged. In other words, we change the aspect ratio of the silicon rectangular posts from 2 to 4. The transmissions at every wavelength show the tendency to first increase and then decrease, while the reflection is just the opposite, as shown in Figs. 6(b) and 6(c). To make it clear, we plot the lines of transmission, reflection, and absorption at the wavelength of 751 nm in Fig. 6(d). Except for the variation of the reflection, the absorption increases as the thickness becomes greater. The transmission reaches its highest at thickness of around 290 nm,

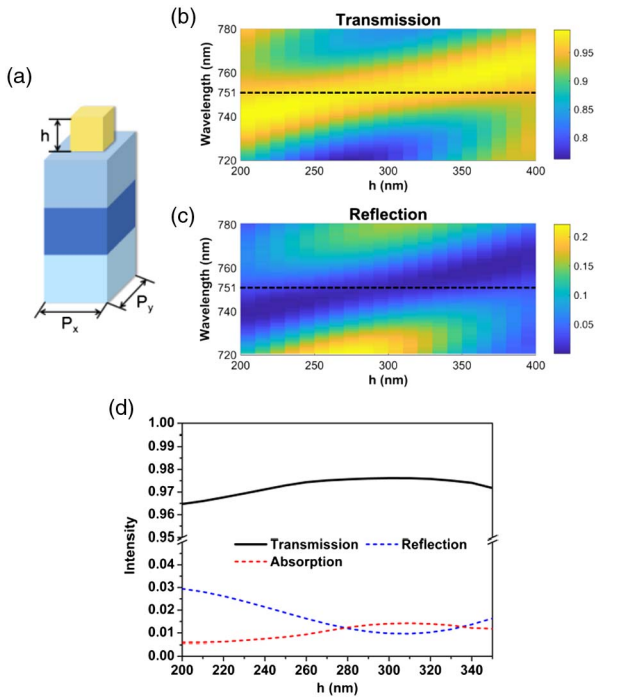

Fig. 6. (a) Schematic of assumptive unit cell composed of rectangular silicon post arrays on quartz substrate. (b), (c) Simulated transmission and reflection of the unit cell with various thickness h of silicon posts for wavelengths of 720–780 nm (the marked dashed lines indicate the variation of transmission and reflection at wavelength of 751 nm). (d) Transmission, reflection, and absorption of the unit cell at wavelength of 751 nm.

which is consistent with previous results. We also change the volume of the rectangular posts, but the result does not show any regularity. Therefore, we attribute the changes of transmission to the influence of the aspect ratio of the silicon posts. We think the transmission of the trapezoid nanoantennas may be the accumulative effect of the small silicon posts.

As we all know, the thickness of the silicon nanoantennas determines the aspect ratio and further determines the etching difficulty. Some methods that can perform high-efficiency beam deflection with low aspect ratios have been studied. Sell *et al.* showed that silicon-based metagratings capable of large-angle multifunctional performance can be realized using an inverse freeform design [39]. They fabricated metagratings that can efficiently deflect light to 75° angles, and the transmission efficiency is above 80%. The method is very novel, which may provide us with a new idea to optimize the designed metasurface in further study. Another work used Huygens' surface to realize high-efficiency beam deflection with low aspect ratios [40]. When spectrally overlapping electric and magnetic dipole resonances of equal strength, the transmission can reach 100% in theory.

C. Larger Refraction Angle

To discuss the properties of the designed metasurface in depth, we analyze the condition of larger anomalous refraction angle θ_r. According to Eq. (8), the refraction angle can be designed by changing the period P_x of the super cell, so we change the period to be 1190 nm, adjust the length l_x of the trapezoid nanoantennas to be 600 nm, and keep other geometrical parameters unchanged at the same time. As is shown in Fig. 7(a), though the transmission efficiency of the desired anomalous refraction is not as good as before, it is still above 60% in the wavelength range of 735–745 nm and up to 76.7% at wavelength of 741 nm, while the anomalous refraction angle is as large as 38.59°, which is shown in Fig. 7(b).

To study the performance of the structure when the anomalous refraction angle becomes larger, we adjust the geometric parameters of the trapezoid structures according to the generalized law of refraction. The anomalous refraction angle is expanded to about 60°. The results show that the total transmission is above 80% in the wavelengths range from 720 to 745 nm, but the anomalous refraction efficiency is only above 45% in this wavelength band. The highest anomalous refraction efficiency is 52% at the wavelength of 733 nm, and the anomalous refraction angle is 57.8°. The section of energy transmitted to redundant diffraction levels is very high, which leads to the limitation of the desired anomalous refraction.

We also test the performance of the structure when the anomalous refraction angle expands to about 80°, but the anomalous refraction efficiency is only about 18%, and most energy is transmitted to redundant diffraction levels, particularly the 0 diffraction level. Therefore, the metasurface basically loses the function of anomalous refraction when the anomalous refraction angle expands to 80°.

4. EXPERIMENTAL FEASIBILITY

Because of limited experimental conditions, the research is based only on numerical simulation. However, silicon has been used in all-dielectric metasurfaces for a long time, and the technology of fabrication is already mature. With support from some reported experimental work [2,3], we discuss the practicable experimental processes. First of all, about 1 μm thick silica can be deposited on a silicon-on-insulator (SOI) wafer comprising a 290 nm thin-film silicon layer on 2 μm of silica by inductively coupled plasma chemical vapor deposition (ICPCVD) technology. Then we spin-coat the adhesive NOA61 and bond the SOI with fused quartz. After it is exposed by ultraviolet light and baked, the upper silicon substrate could be removed by polishing and deep reactive ion etching (DRIE). Then, by removing the upper silica layer by HF acid, the silicon film on quartz substrate could be obtained. Finally, electron beam lithography (EBL) and inductively coupled plasma (ICP) technology could be used to obtain the pattern. In addition, during the lithography process, we could use a thin aluminum (Al) or chromium (Cr) layer as the resist.

Considering that the side length w_1 of the trapezoidal structure is fixed at 82 nm, which may be difficult to precisely fabricate, we calculate the total transmission and desired anomalous refraction efficiency at different values of w_1 to test the tolerance of the structure. As shown in Fig. 8, when w_1 becomes longer, the total transmission and anomalous refraction efficiency at a wavelength of 751 nm show a downward trend, but the transmissions at a wavelength of around 775 nm become higher. When $w_1 = 100$ nm, the total transmission is

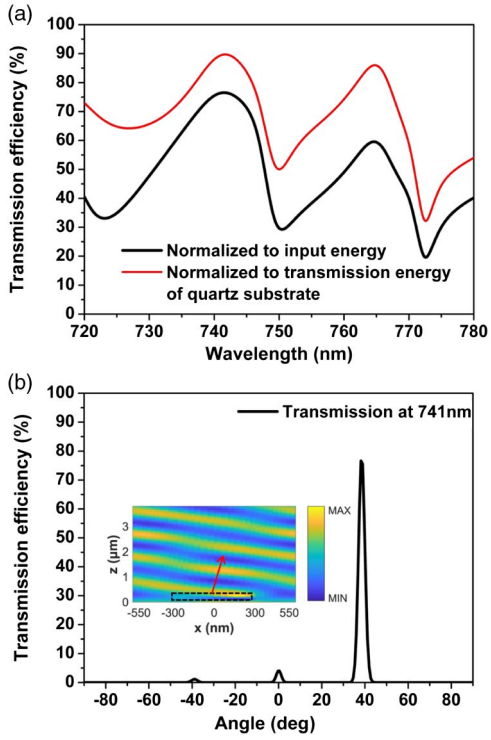

Fig. 7. Transmission efficiency with the fixed geometric parameters of the silicon trapezoidal antennas. (a) Simulated transmission efficiency normalized to input energy and the transmission energy of the quartz substrate for wavelengths of 720–780 nm, and (b) far-field transmission efficiency (normalized to input energy) for different anomalous refraction angles (θ_r).

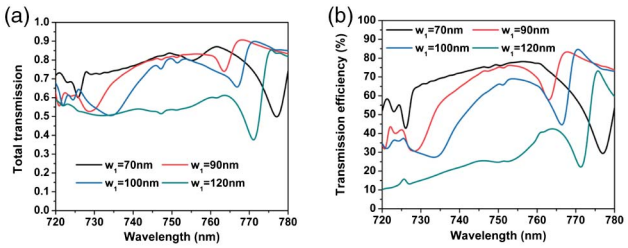

Fig. 8. (a) Calculated total transmission at different values of w_1. (b) Calculated desired anomalous refraction efficiency at different values of w_1.

up to 77.5% and the desired anomalous refraction efficiency is still as high as 65%, but when w_1 increases to 120 nm, the total transmission is only 53.3% and the anomalous refraction efficiency is only 25.5%. In addition, as shown in Fig. 8(b), when $w_1 = 100$ nm, the anomalous refraction efficiency is up to 85.5% at wavelength of 770 nm.

In conclusion, when w_1 changes from 70 to 90 nm, the transmission efficiency of the metasurface is almost constant. When w_1 is 100 nm, the transmission efficiency can also remain at a high level.

5. CONCLUSION

An efficient all-dielectric metasurface based on quasi-continuous trapezoidal silicon nanoantennas arranged on a quartz substrate is designed and simulated. Compared to conventional metasurfaces based on arrays of discrete silicon posts, due to the asymmetry of the trapezoidal nanoantennas, the designed quasi-continuous metasurface has polarization selectivity. Only light with direction of polarization perpendicular to the direction of the phase gradient can produce a full 2π linear phase gradient. The results also show that the operation wavelength band is moving. This may provide a new idea for designing all-dielectric phase-gradient metasurfaces. The simulation results show that full 2π phase shift is realized and the total transmission reaches 88.0%. The efficiency of the desired anomalous refraction is up to 80.4%, while the transmission angle is 29.62° at the wavelength of 751 nm. The metasurface has a certain operating bandwidth of about 40 nm from 740 to 780 nm in which the desired anomalous refraction efficiency is above 70%. This means our metasurface does not have to work at an accurate operating wavelength. Also, we can gain larger refraction angles by tailoring the period of the super cell while the transmission efficiency is still high. The metasurface achieves simple structure, high efficiency, and large anomalous refraction angle at the same time. We think it can lay the foundation for future research of transmission mode metasurfaces that can be fabricated on a large scale. The designed metasurface could be further applied to all-important integrated optical devices, especially flat lenses.

Funding. National Key R&D Program of China (2016YFA0301300); National Natural Science Foundation of China (NSFC) (61275201, 61372037); BUPT Excellent Ph.D. Students Foundation (CX2016204, CX2017401); Fundamental Research Funds for the Central Universities (2016RC24); Fund of State Key Laboratory of Information Photonics and Optical Communications (IPOC20172204).

†These authors contributed equally to this work.

REFERENCES

1. L. Zhang, S. Mei, K. Huang, and C. W. Qiu, "Advances in full control of electromagnetic waves with metasurfaces," Adv. Opt. Mater. **4**, 818–833 (2016).
2. Z. Zhou, J. Li, R. Su, B. Yao, H. Fang, K. Li, L. Zhou, J. Liu, D. Stellinga, C. P. Reardon, and T. F. Krauss, "Efficient silicon metasurfaces for visible light," ACS Photon. **4**, 544–551 (2017).
3. M. I. Shalaev, J. Sun, A. Tsukernik, A. Pandey, K. Nikolskiy, and N. M. Litchinitser, "High-efficiency all-dielectric metasurfaces for ultracompact beam manipulation in transmission mode," Nano Lett. **15**, 6261–6266 (2015).
4. Y. Zhao, X. Cao, J. Gao, X. Liu, and S. Li, "Jigsaw puzzle metasurface for multiple functions: polarization conversion, anomalous reflection and diffusion," Opt. Express **24**, 11208–11217 (2016).
5. W. Zhu, F. Xiao, M. Kang, and M. Premaratne, "Coherent perfect absorption in an all-dielectric metasurface," Appl. Phys. Lett. **108**, 121901 (2016).
6. N. Yu, P. Genevet, M. A. Kats, F. Aieta, J. P. Tetienne, F. Capasso, and Z. Gaburro, "Light propagation with phase discontinuities: generalized laws of reflection and refraction," Science **334**, 333–337 (2011).
7. N. Yu, F. Aieta, P. Genevet, M. A. Kats, Z. Gaburro, and F. Capasso, "A broadband, background-free quarter-wave plate based on plasmonic metasurfaces," Nano Lett. **12**, 6328–6333 (2012).
8. X. Ni, N. K. Emani, A. V. Kildishev, A. Boltasseva, and V. M. Shalaev, "Broadband light bending with plasmonic nanoantennas," Science **335**, 427 (2012).
9. Z. Liu, Q. Wang, Y. Xie, and Y. Zhu, "High-efficiency control of transmitted light with a three-layered plasmonic metasurface," J. Phys. D **49**, 475101 (2016).
10. T. Li, L. Huang, J. Liu, Y. Wang, and T. Zentgraf, "Tunable wave plate based on active plasmonic metasurfaces," Opt. Express **25**, 4216–4226 (2017).
11. X. Ni, A. V. Kildishev, and V. M. Shalaev, "Metasurface holograms for visible light," Nat. Commun. **4**, 2807 (2013).
12. X. Chen, H. Zhou, M. Liu, and J. Dong, "Measurement of orbital angular momentum by self-interference using a plasmonic metasurface," IEEE Photon. J. **8**, 4800308 (2016).
13. S. Sun, Z. Zhou, C. Zhang, Y. Gao, Z. Duan, S. Xiao, and Q. Song, "All-dielectric full-color printing with TiO_2 metasurfaces," ACS Nano **11**, 4445–4452 (2017).
14. M. Khorasaninejad, A. Ambrosio, P. Kanhaiya, and F. Capasso, "Broadband and chiral binary dielectric meta-holograms," Sci. Adv. **2**, e1501258 (2016).
15. B. Wang, F. Dong, Q. T. Li, D. Yang, C. Sun, J. Chen, Z. Song, L. Xu, W. Chu, Y. F. Xiao, and Q. Gong, "Visible-frequency dielectric metasurfaces for multiwavelength achromatic and highly dispersive holograms," Nano Lett. **16**, 5235–5240 (2016).
16. Z. Y. Li, M. H. Kim, C. Wang, Z. H. Han, S. Shrestha, A. C. Overvig, M. Lu, A. Stein, A. M. Agarwal, M. Lončar, and N. F. Yu, "Controlling propagation and coupling of waveguide modes using phase-gradient metasurfaces," Nat. Nanotechnol. **12**, 675–683 (2017).
17. M. Chen, J. Cai, W. Sun, L. Chang, and X. Xiao, "High-efficiency all-dielectric metasurfaces for broadband polarization conversion," Plasmonics **13**, 21–29 (2016).
18. F. Ding, Z. Wang, V. M. Shalaev, and A. V. Kildishev, "Broadband high-efficiency half-wave plate using plasmonic metasurface," in *CLEO: QELS_Fundamental Science* (Optical Society of America, 2015), paper FTu1C.6.

19. H. S. Ee and R. Agarwal, "Tunable metasurface and flat optical zoom lens on a stretchable substrate," Nano Lett. **16**, 2818–2823 (2016).
20. S. Wang, J. Lai, T. Wu, C. Chen, and J. Sun, "Wide-band achromatic flat focusing lens based on all-dielectric subwavelength metasurface," Opt. Express **25**, 7121–7130 (2017).
21. M. Khorasaninejad, A. Y. Zhu, C. Roques-Carmes, W. T. Chen, J. Oh, I. Mishra, R. C. Devlin, and F. Capasso, "Polarization-insensitive metalenses at visible wavelengths," Nano Lett. **16**, 7229–7234 (2016).
22. M. Khorasaninejad, W. T. Chen, R. C. Devlin, J. Oh, A. Y. Zhu, and F. Capasso, "Metalenses at visible wavelengths: diffraction-limited focusing and subwavelength resolution imaging," Science **352**, 1190–1194 (2016).
23. A. Zhan, S. Colburn, R. Trivedi, T. K. Fryett, C. M. Dodson, and A. Majumdar, "Low-contrast dielectric metasurface optics," ACS Photon. **3**, 209–214 (2016).
24. K. E. Chong, I. Staude, A. James, J. Dominguez, S. Liu, S. Campione, G. S. Subramania, T. S. Luk, M. Decker, D. N. Neshev, and I. Brener, "Polarization-independent silicon metadevices for efficient optical wavefront control," Nano Lett. **15**, 5369–5374 (2015).
25. Z. Li and K. Aydin, "Broadband metasurfaces for anomalous transmission and spectrum splitting at visible frequencies," EPJ Appl. Metamater. **2**, 2 (2015).
26. S. Gao, W. Yue, C. S. Park, S. S. Lee, E. S. Kim, and D. Y. Choi, "Aluminum plasmonic metasurface enabling a wavelength-insensitive phase gradient for linearly polarized visible light," ACS Photon. **4**, 322–328 (2017).
27. Z. Li, E. Palacios, S. Butun, and K. Aydin, "Ultrawide angle, directional spectrum splitting with visible-frequency versatile metasurfaces," Adv. Opt. Mater. **4**, 953–958 (2016).
28. Z. Li, E. Palacios, S. Butun, and K. Aydin, "Visible-frequency metasurfaces for broadband anomalous reflection and high-efficiency spectrum splitting," Nano Lett. **15**, 1615–1621 (2015).
29. S. Sun, K. Y. Yang, C. M. Wang, T. K. Juan, W. T. Chen, C. Y. Liao, Q. He, S. Xiao, W. T. Kung, G. Y. Guo, and L. Zhou, "High-efficiency broadband anomalous reflection by gradient meta-surfaces," Nano Lett. **12**, 6223–6229 (2012).
30. G. Zheng, H. Mühlenbernd, M. Kenney, G. Li, T. Zentgraf, and S. Zhang, "Metasurface holograms reaching 80% efficiency," Nat. Nanotechnol. **10**, 308–312 (2015).
31. C. Pfeiffer and G. Anthony, "Metamaterial Huygens' surfaces: tailoring wave fronts with reflectionless sheets," Phys. Rev. Lett. **110**, 197401 (2013).
32. Y. Sun, G. C. Welch, W. L. Leong, C. J. Takacs, G. C. Bazan, and A. J. Heeger, "Solution-processed small-molecule solar cells with 6.7% efficiency," Nat. Mater. **11**, 44–48 (2012).
33. M. A. Otte, A. Garcia-Martin, X. Borrise, and B. Sepulveda, "Metamirrors based on arrays of silicon nanowires with height gradients," Adv. Opt. Mater. **5**, 1600933 (2017).
34. Z. Li, L. Huang, K. Lu, Y. Sun, and L. Min, "Continuous metasurface for high-performance anomalous reflection," Appl. Phys. Express **7**, 112001 (2014).
35. A. B. Evlyukhin, R. L. Eriksen, W. Cheng, J. Beermann, C. Reinhardt, A. Petrov, S. Prorok, M. Eich, B. N. Chichkov, and S. I. Bozhevolnyi, "Optical spectroscopy of single Si nanocylinders with magnetic and electric resonances," Sci. Rep. **4**, 4126 (2014).
36. D. Sell, J. Yang, S. Doshay, K. Zhang, and J. A. Fan, "Visible light metasurfaces based on single-crystal silicon," ACS Photon. **3**, 1919–1925 (2016).
37. E. D. Palik, *Handbook of Optical Constants of Solids* (Academic Press, 1985).
38. S. Larouche and D. R. Smith, "Reconciliation of generalized refraction with diffraction theory," Opt. Lett. **37**, 2391–2393 (2012).
39. D. Sell, J. Yang, S. Doshay, R. Yang, and J. A. Fan, "Large-angle, multifunctional metagratings based on freeform multimode geometries," Nano Lett. **17**, 3752–3757 (2017).
40. M. Decker, I. Staude, M. Falkner, J. Dominguez, D. N. Neshev, I. Brener, T. Pertsch, and Y. S. Kivshar, "High-efficiency dielectric Huygens' surfaces," Adv. Opt. Mater. **3**, 813–820 (2015).